

The Chiton Stylus Canal: An Element Delivery Pathway for Tooth Cusp Biomineralization

Jeremy A. Shaw,^{1*} David J. Macey,² Lesley R. Brooker,³ Edward J. Stockdale,¹ Martin Saunders,¹ and Peta L. Clode¹

¹Centre for Microscopy, Characterisation and Analysis, The University of Western Australia, Crawley, WA 6009, Australia

²School of Biological Sciences and Biotechnology, Murdoch University, Murdoch, WA 6150, Australia

³Faculty of Science, Health and Education, University of the Sunshine Coast, Maroochydore DC, Queensland 4558, Australia

ABSTRACT A detailed investigation of the stylus canal situated within the iron mineralized major lateral teeth of the chiton *Acanthopleura hirtosa* was undertaken in conjunction with a row-by-row examination of cusp mineralization. The canal is shown to contain columnar epithelial tissue similar to that surrounding the mineralized cusps, including the presence of iron rich particles characteristic of the iron storage protein ferritin. Within the tooth core, a previously undescribed internal pathway or plume is evident above the stylus canal, between the junction zone and mineralizing posterior face of the cusp. Plume formation coincides with the appearance of iron in the superior epithelium and the onset of mineralization at tooth row 13. The plume persists during the delivery of phosphorous and calcium into the tooth core, and is the final region of the cusp to become mineralized. The presence of the stylus canal was confirmed in a further 18 chiton species, revealing that the canal is common to polyplacophoran molluscs. These new data strongly support the growing body of evidence highlighting the importance of the junction zone for tooth mineralization in chiton teeth, and indicate that the chemical and structural environment within the tooth cusp is under far greater biological control than previously considered. *J. Morphol.* 270: 588–600, 2009. © 2008 Wiley-Liss, Inc.

KEY WORDS: SEM; X-ray microanalysis; EDS; TEM; EFTEM; microwave; iron; magnetite; mollusk; radula

INTRODUCTION

Chitons (Mollusca: Polyplacophora) utilize a range of iron and calcium-based minerals to harden their teeth, which allows them to graze upon algae growing on, or within, hard substrates (Lowenstam, 1962). In particular, the iron oxide magnetite is used to structurally reinforce the posterior surface of each major lateral tooth cusp. Despite this hardening process, the abrasive nature of their feeding activities quickly wears down the teeth, making it necessary for them to be continually replaced (Runham and Thornton, 1967; Shaw et al., 2008a). The organ involved in the synthesis, development, and eventual loss of the teeth is

termed the radula; an elongated ribbon of repeating tooth rows that moves progressively toward the mouth in a manner analogous to a production line. Each tooth row consists of 17 teeth, 16 of which are paired either side of a single central tooth. The major laterals (also referred to as second laterals) are the only tooth pair that are mineralized using iron and calcium. Initially, the teeth form at the posterior end of the radula, where odontoblast cells construct an extracellular organic matrix, composed primarily of the polysaccharide α -chitin (Evans et al., 1990). This matrix acts as a scaffold that dictates the overall structure of the teeth and plays an important functional role as they progress from the unmineralized to the mineralized state.

One of the most intriguing and well-studied aspects of tooth formation in chitons is the highly ordered internal structure of each tooth cusp, where various mineral types are separated into architecturally discrete regions (see Fig. 1). The composite structure of the teeth provides a number of functional benefits that prolong the working life of each cusp, including shock absorbance, minimizing crack propagation, and the ability to self sharpen (van der Wal et al., 2000). Although tooth formation in chitons represents a classic example of extracellular matrix-mediated biomineralization, the mechanisms involved in the controlled formation of these discrete mineral phases are not well understood.

During development, the major lateral tooth cusps are surrounded by superior epithelial tissue (cusp epithelium), which is thought to be the main

Contract grant sponsor: Australian Research Council Discovery Grant; Contract grant number: DP0559858.

*Correspondence to: Jeremy A. Shaw, CMCA (M010), The University of Western Australia, 35 Stirling Highway, Crawley, WA 6009, Australia. E-mail: jeremy.shaw@uwa.edu.au

Published online 23 December 2008 in Wiley InterScience (www.interscience.wiley.com)
DOI: 10.1002/jmor.10705

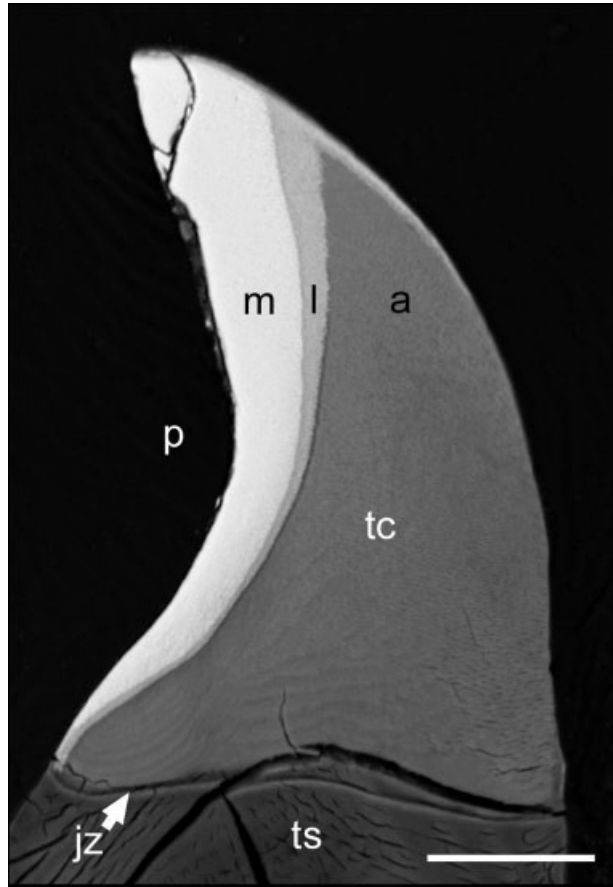


Fig. 1. Back-scattered SEM micrograph of a longitudinal section through a major lateral tooth from *Acanthopleura hirtosa*, highlighting the overall internal structure of a mature tooth including the tooth base or stylus (ts), junction zone (jz), and tooth cusp (tc). In addition, the cusp is further divided into distinct mineral regions, which include magnetite (m), lepidocrocite (l), and apatite (a). p, posterior surface. Scale bar = 50 μm .

route of delivery for elements involved in the mineralization process. However, there is a growing body of evidence to suggest that the supply of elements for tooth mineralization in chitons is derived from two sources (Macey and Brooker, 1996; Brooker et al., 2003). The first is the direct cellular transport of elements stored within the cusp epithelium, while the second is via a pool of elements that accumulate at an interface between the tooth cusp and base, termed the junction zone (see Fig. 1). To date, no attempts have been made to ascertain how elements are delivered and selectively stored at the junction zone or how they are subsequently delivered into the tooth cusps.

Despite the wealth of literature available on tooth cusp mineralization, very little work has been conducted on the major lateral tooth bases (also referred to as the tooth stylus in many anatomical manuscripts). In particular, the role of a curious tube-like tissue filled cavity within the major lateral tooth stylus has remained unde-

scribed. The presence of this structure was first reported by Nesson and Lowenstam (1985), however no suggestions were raised as to its possible function.

An investigation of the major lateral tooth bases of the chiton *Acanthopleura hirtosa* was undertaken to determine both the overall morphology of the stylus canal and the nature of the cells located within the canal. In addition, the major lateral teeth from a number of other chiton species were examined to determine whether the canal is a feature common to this class of molluscs. To elucidate links between the junction zone and tooth cusp mineralization, a detailed row-by-row investigation of mineral deposition within the major lateral teeth was also conducted. In this article, evidence is provided that strongly supports the involvement of the stylus canal in tooth cusp mineralization and its role in element transfer between the junction zone and tooth core.

MATERIALS AND METHODS

The Stylus Canal

Adult specimens of the chiton *Acanthopleura hirtosa* (Blainville, 1825) were collected from Woodman Point, Perth, on Australia's south-west coast (Lat. 32°S, Long. 116°E). For investigations of gross stylus canal morphology, excised radulae were cleaned in 2% sodium hypochlorite (5 min) and then rinsed in distilled water to remove the epithelial tissue attached to the teeth. Whole radulae, radula segments, individual major lateral teeth, and fractured teeth were either imaged on a dissecting microscope (Olympus, SZH10) fitted with a digital camera (Olympus, DP10) or processed further for scanning electron microscopy (SEM). For SEM, radulae were fixed for at least 12 h in 2.5% glutaraldehyde buffered in seawater before being dehydrated through a graded series of ethanol followed by amyl acetate. Samples were critical point dried with CO_2 , mounted on aluminum stubs using double-sided carbon tape, and then coated with 30 nm gold before SEM imaging (Philips, XL 20) at 10 kV.

For the superior epithelium and stylus canal tissue, radulae were dissected and then processed using a microwave-assisted protocol as described in Shaw et al. (2008b). Briefly, radulae were excised from freshly collected specimens and then immediately bathed in 2.5% glutaraldehyde buffered in 0.1 M phosphate at pH 7.2 (osmotic pressure adjusted to 900 mmol kg^{-1} using sucrose) before further fixation, dehydration, and infiltration in a laboratory microwave (Pelco, Biowave[®]). Once polymerized, resin blocks were oriented to provide transverse and longitudinal sections of the stylus canal, which were cut to a thickness of $\sim 1 \mu\text{m}$ and $\sim 100 \text{ nm}$ for light microscopy (LM) and transmission electron microscopy (TEM), respectively. For LM, sections mounted on glass slides were stained with 1% Methylene Blue + 1% Azur II (aqueous) for 20 s and imaged on an optical microscope (Olympus, BX51) fitted with a digital camera (Olympus, DP70). For TEM, sections mounted on formvar-film copper grids were double stained with uranyl nitrate (10 min) and Sato's lead citrate (10 min) (Hanaichi et al., 1986) and imaged on a TEM (JEOL, 2000FX) with plate film at 80 kV.

For energy-filtered TEM imaging and analysis, unstained sections ($\sim 100 \text{ nm}$ thick) were mounted on copper grids and analyzed at 200 kV in a TEM (JEOL, 2100), fitted with a Gatan Imaging Filter (GIF, Tridiem). Bright-field TEM images were taken before obtaining elemental maps for iron, which were acquired using the iron M-edge and generated using the conventional three-window method (see, Brydson, 2001). Two pre-

TABLE 1. *Chiton* species in which the major lateral tooth bases were investigated for the presence of the stylus canal

Species			Collection site	Lat	Long
	Order Lepidopleurida Suborder Lepidopleurina				
Family Leptochitonidae	<i>Leptochiton liratus</i>	(Adams and Angas, 1864)	Cottesloe Reef, WA.	31°60'S	115°45'E
	Order Chitonida Suborder Chitonina				
Family Callistoplacidae	<i>Callochiton crocinus</i>	(Reeve, 1847)	Cottesloe Reef, WA.	31°60'S	115°45'E
	<i>Ischnochiton cariosus</i>	(Carpenter in Pilsbry, 1892)			
	<i>Ischnochiton contractus</i>	(Reeve, 1847)			
Family Ischnochitonidae	<i>Ischnochiton torri</i>	(Iredale and May, 1916)	Hamelin Bay, WA.	34°11'S	115°01'E
	<i>Ischnochiton verconis</i>	(Torr, 1911)			
Family Chitonidae	<i>Ischnochiton thomasi</i>	(Bednall, 1897)	Cottesloe Reef, WA.	31°60'S	115°45'E
	<i>Rhyssoplax torriana</i>	(Hedley and Hull, 1910)	Port Headland, WA.	20°18'S	118°36'E
	<i>Acanthopleura gemmata</i>	(Blainville, 1825)			
	<i>Acanthopleura spinosa</i>	(Bruguière, 1792)	Woodman Point, WA	32°03'S	115°44'E
	<i>Acanthopleura hirtosa</i>	(Blainville, 1825)	Rottneest Is., WA	31°59'S	115°32'E
	<i>Onithochiton quercinus</i>	(Gould, 1846)			
	Suborder Acanthochitonina				
Family Cryptoplacidae	<i>Cryptoplax burrowi</i>	(E.A. Smith, 1884)	Cottesloe Reef, WA.	31°60'S	115°45'E
	<i>Cryptoplax iredalei</i>	(Ashby, 1923)			
	<i>Cryptoplax striata</i>	(Lamarck, 1819)			
Family Mopaliidae	<i>Plaxiphora matthewsi</i>	(Iredale, 1910)	Woodman Point, WA.	32°03'S	115°44'E
	<i>Plaxiphora albida</i>	(Blainville, 1825)			
Family Acanthochitonidae	<i>Acanthochitona johnstoni</i>	(Ashby, 1923)	Monterey Bay, USA	36°45'N	122°0'W
	<i>Cryptochiton stelleri</i>	(Middendorff, 1847)			

Solid vertical lines denote groups of species from the same family, whereas dashed vertical lines denote groups of species collected from the same site.

edge (background) images were acquired at energies of 45 and 50 eV, and the postedge (signal energy) image was acquired by centering the GIF's energy-selecting slit at 59 eV with a slit width of 5 eV (15 s acquisition time). We used 4× binning to obtain suitable signal-to-noise levels.

To confirm whether the stylus canal is present in other chitons, the major lateral teeth of an additional 18 chiton species (Table 1) were investigated at the LM level. A minimum of two individuals were examined for each species.

Cusp Mineralization

Longitudinal sections of the radula, with the superior epithelium left intact, were prepared for LM as outlined above, with the exception that sections were stained for ferric iron using a variation of the Perl's Prussian blue method (Culling, 1974). Resin sections were stained for 15 min in a freshly prepared solution comprised of equal parts of potassium ferrocyanide and hydrochloric acid, each made to 4% (w/v) in distilled water.

For SEM, radulae were excised from freshly collected specimens and cleaned using a fine water jet to remove the epithelial tissue surrounding the tooth cusps. To accurately record the number of tooth rows within each developmental stage, radulae were photographed using the optical microscope system outlined above. Radulae were then fixed overnight using 2.5% glutaraldehyde buffered in 0.1 M phosphate at pH 7.2 (osmotic pressure adjusted to 900 mmol kg⁻¹ using sucrose) (Shaw et al., 2008b), before dehydration through a graded series of ethanol followed by propylene oxide.

A two-step embedding method was used to obtain precise longitudinal orientations along each radula. Dehydrated specimens were first infiltrated and embedded using Procure-Araldite resin, and, following polymerization in an oven at 60°C overnight, sample blocks were trimmed such that the face of the block revealed a longitudinal section along the radula. Once orientated, samples were placed in aluminum ring molds and re-embedded in Procure-Araldite. Sagittal sections through the major lateral teeth were obtained by polishing these samples with a graded series of Struers silicon carbide papers up to

4000 grit. The final polishing step was performed with 1 µm diamond paste before coating with 30 nm carbon.

For SEM imaging and X-ray microanalysis (EDS), polished samples were examined in a field emission SEM (Zeiss VP-1555) fitted with an X-ray analytical system (Oxford Instruments, INCA x-sight) with thin window detector. For EDS, qualitative spectral data and element maps were collected at an accelerating voltage of 20 kV, with a beam current of 1 nA and an optimal working distance of 16 mm. The EDS system was calibrated with a copper standard before sample analysis, and at 2 h intervals thereafter.

All numerical data are presented as mean ± 1 standard deviation, where n = the number of animals.

RESULTS

The Stylus Canal

For each tooth row, which consists of nine tooth types, the stylus canal was found only within the major lateral teeth of all chiton species examined (Table 1). In *Acanthopleura hirtosa*, the major lateral teeth are supported by a tooth base (stylus) measuring ~540 µm in length and ~360 µm in height (see Fig. 2), which is embedded in the radula membrane. When excised from this membrane the stylus canal was clearly seen within the tooth stylus (see Fig. 2). Located centrally on the medial surface of the stylus, a teardrop-shaped canal pore, 100 µm across, opens into the stylus canal (Figs. 2 and 3), extends ~280 µm into the stylus toward the distal end of the tooth and ends blindly ~25 µm below the junction zone (Figs. 2 and 3). This arm of the canal tapers from ~75 µm at the pore opening to ~25 µm at the end adjacent

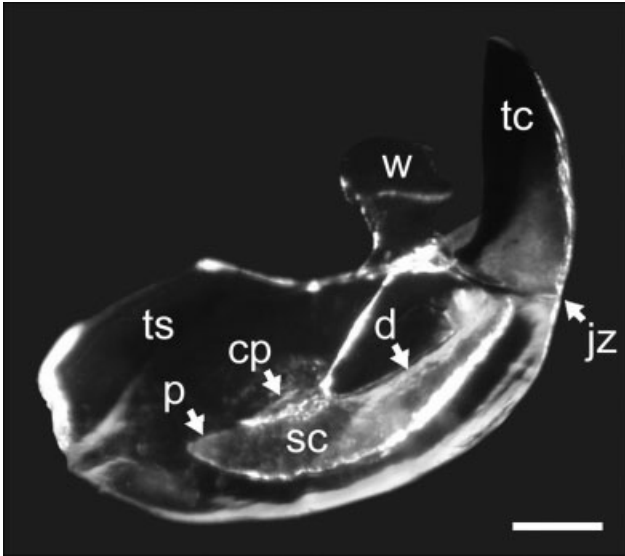


Fig. 2. Medial surface of a major lateral tooth freshly dissected from the chiton *Acanthopleura hirtosa* highlighting the distal (d) and proximal (p) arms of the stylus canal (sc), which stem from the canal pore (cp) on the medial face of the tooth stylus (ts). tc, tooth cusp; jz, junction zone; w, major lateral wing. Scale bar = 100 μm .

to the junction zone. The stylus canal also extends $\sim 125 \mu\text{m}$ toward the proximal end of the tooth.

Light microscopy showed that the stylus canal and the canal pore were filled with tissue similar to that surrounding the major lateral and minor teeth (Fig. 4A,B). Within the distal region of the canal, prominent nuclei were observed $\sim 30 \mu\text{m}$ from the apical pole of each cell. Dark staining granules were also present within the apical region of the canal tissue (Fig. 4B). When observed using TEM, the ultrastructure of the canal cells is consistent with columnar epithelium (see Fig. 5), and is highly comparable to the superior epithelium that surrounds the mineralizing surfaces of the major lateral teeth. A well-developed system of rough endoplasmic reticulum is situated apically to the nuclei, which is adjacent to numerous electron dense bodies that are likely to represent the dark staining granules observed by LM (Fig. 5A,B). Numerous mitochondria were also visible, and at the apical pole of each cell, a series of interdigitating membranes was observed that border the surface of the canal (Fig. 5C). Notably, these interdigitating membranes were found only at the distal end of the canal, where the cells abut the surface closest to the junction zone. Junctional complexes, common to epithelial cells, were also evident in the cell membrane near the apical terminus of each cell (Fig. 5C).

The electron density and structure of granules within the apical region was highly variable, with some granules containing dense inclusions or an outer layer of dense material, while others are

membrane bound. At higher magnification, TEM images and energy-filtered TEM iron maps depict the presence of 8 nm iron particles, which were observed individually and in aggregations throughout the apical cytoplasm of the canal cells (Fig. 6A–C). The size of these particles is consistent with the iron core of ferritin (Lewin et al., 2005).

Cusp Mineralization

Radulae of *A. hirtosa* exhibit a high degree of consistency with respect to the pattern of mineralization of their major lateral tooth cusps. Overall, radulae have 73 ± 3 ($n = 12$) transverse tooth rows, which can be divided into a number of visually distinct stages, most of which occur early in development as the teeth progress from the unmineralized to the mineralized state. Stage 1 teeth (rows 1 to 10 ± 1) are clear and unmineralized, Stage 2 teeth (rows 11 to 13 ± 0) are yellow, Stage 3 (row 14 ± 0) is comprised of a single dark orange tooth, and in Stage 4 (rows 15 to 73 ± 3), the teeth are black capped.

Back scattered electron imaging of longitudinal sections of the radula reveal a series of anteriorly intensifying bands of high atomic number material at the junction zone. Qualitative spectral data from the junction zone indicate that sulfur is present at tooth row 7 followed by the appearance of iron, phosphorous, calcium, and magnesium at tooth row 8. Mineralization of the tooth cusps is initiated at row 13, as evidenced by the deposition of small electron dense crystals along the fibers of the organic matrix (see Fig. 7). Sections stained for ferric iron (Fe^{3+}) also reveal a dramatic increase in the number of iron containing granules (siderosomes) within the apical cusp epithelium on both the anterior and posterior surfaces of the cusps at row 13 (see Fig. 8). A limited number of siderosomes are also present from tooth rows 7 to 12 (Fig. 8A,B). As with the individual particles and aggregations of iron in the canal cells, these siderosomes comprise 8 nm particles of iron (see Fig. 9).

Also at row 13, Perl's staining revealed the presence of a previously undescribed plume of iron within the tooth core between the junction zone and the iron mineralizing region (see Fig. 8). The plume extends toward the cusp tip $\sim 30 \mu\text{m}$ from the posterior cusp surface, coinciding with the anterior boundary of the developing magnetite region. The plume was also evident when the cusps are observed using back-scattered electrons in the SEM, with EDS confirming the presence of iron in this region (see Fig. 10). Phosphorus and calcium were also detected both within the junction zone and the posterior iron mineralizing region of the cusp (see Fig. 10).

The plume was observed in all subsequent stages of tooth development following the onset of

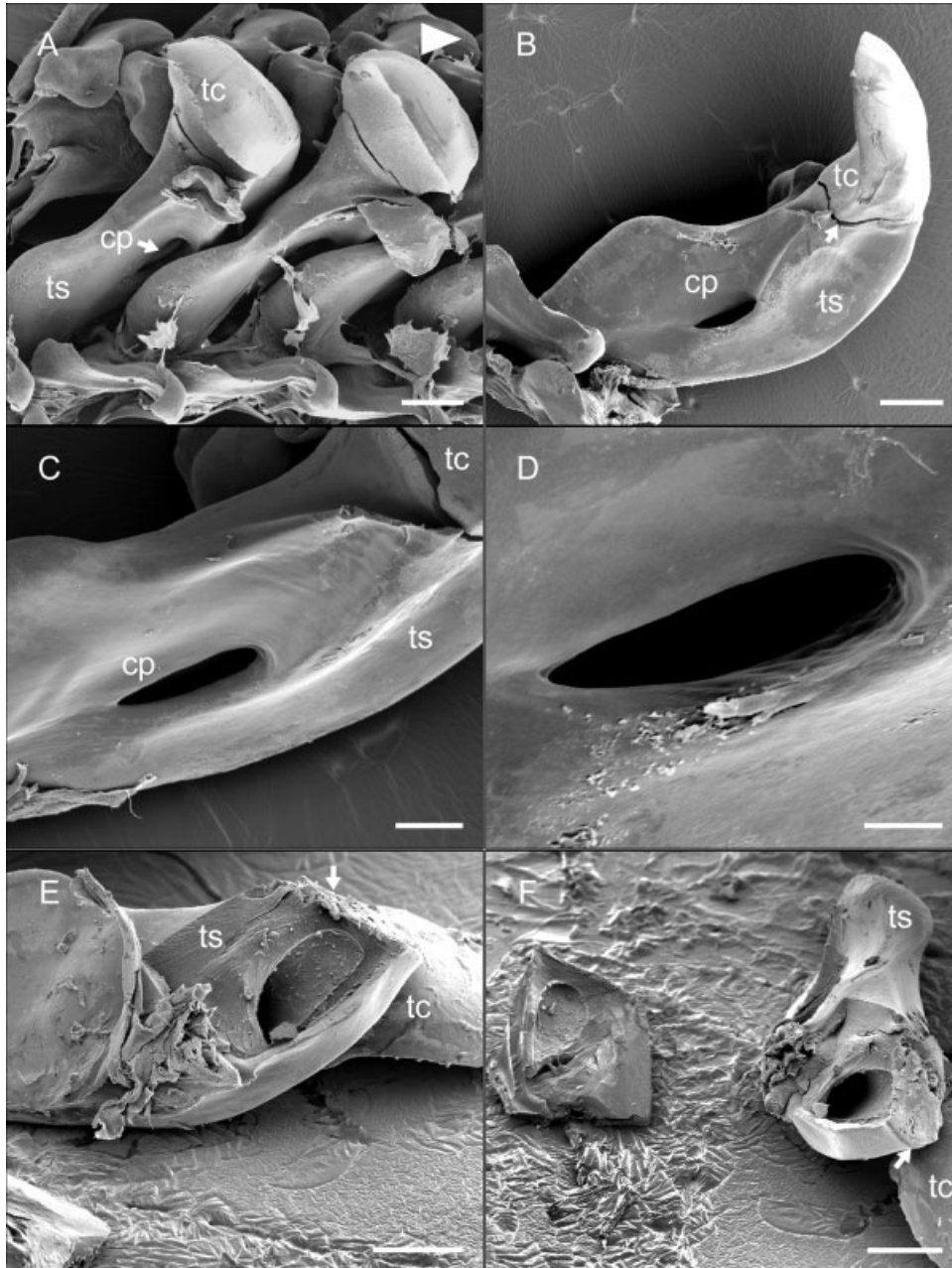


Fig. 3. Whole and fractured major lateral teeth from the chiton *Acanthopleura hirtosa*. **A:** The relative position of the canal pore (cp) on the medial surface of the tooth stylus (ts). Arrowhead denotes anterior direction. Scale bar = 100 μm . **B:** Medial tooth surface, highlighting the central position of the canal pore on the tooth stylus. Arrow denotes a fracture at the junction zone. Scale bar = 100 μm . **C and D:** Higher magnification images of the canal pore. Scale bars = (C) 50 μm and (D) 25 μm . **E and F:** Fractured stylus, with tooth cusp (tc) removed, exposing the distal arm of the stylus canal and highlighting the close proximity of the canal to the junction zone region (arrow). Scale bars = 100 μm .

iron mineralization. These stages include the formation of the lepidocrocite layer at row 31 ± 1 ($n = 6$) (see Fig. 11) and apatite mineralization of the tooth core at row 37 ± 2 ($n = 4$) (see Fig. 12). In addition to iron, phosphorous and calcium were also observed within the plume region during core mineralization. The apatite mineralization front

migrates ventrally along the boundary of the iron mineralized region and anterior cusp surface, before progressively infilling the remainder of the core, which is predominantly mineralized by row 47 ± 3 ($n = 4$) (see Fig. 12). The final region of the core to mineralize is where the plume extends from the junction zone to the lepidocrocite layer (see Fig. 13).

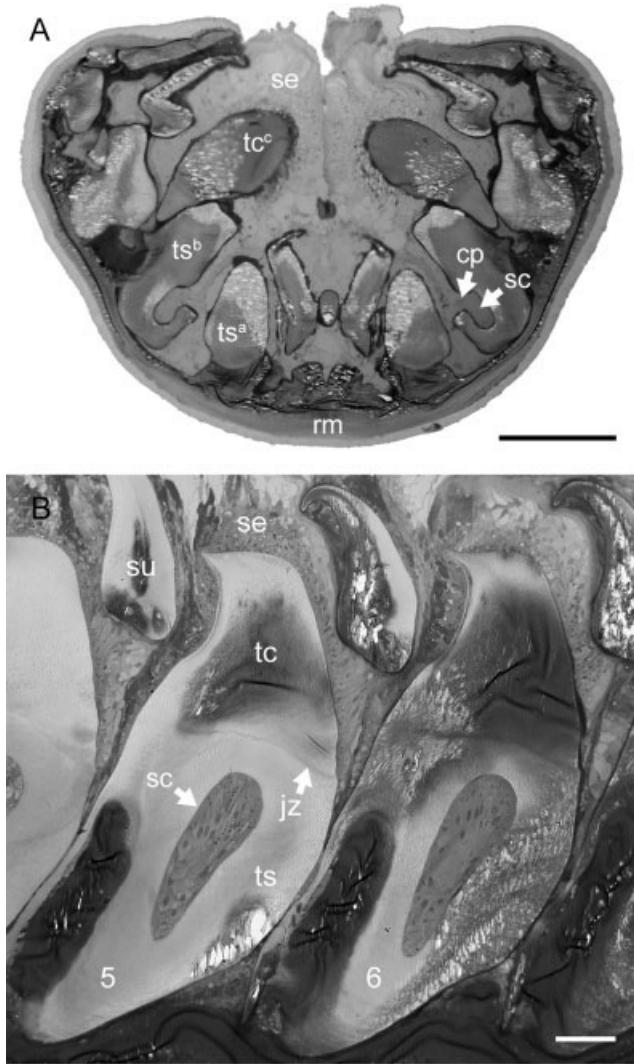


Fig. 4. Stylus canal tissue within the major lateral tooth bases of the chiton *Acanthopleura hirtosa*. **A:** In transverse section at row 10, three overlapping major lateral tooth rows (a, b, and c) are visible due to the interlocking nature of the teeth. The tooth stylus (ts) at row (b) shows the canal pore (cp) opening into the stylus canal (sc), which is filled with epithelial tissue. Scale bar = 200 μ m. **B:** In longitudinal section at rows 5 and 6, prominent nuclei and other organelles can be seen within the cells of the canal, which terminates \sim 25 μ m from the junction zone (jz). Scale bar = 50 μ m. rm, radula membrane; se, superior epithelium.

The position of the plume coincides with differences in structural organization within the tooth cusp. When observed using TEM, the fibers of the organic matrix in the plume region appear to cross from the tooth stylus to the junction zone and into the cusp (Fig. 14A). In mature teeth, back-scattered SEM images reveal a discontinuity in tooth structure in the plume region above the stylus canal (Fig. 14B), represented by a break in the layered substructure of the core (Fig. 14A,B).

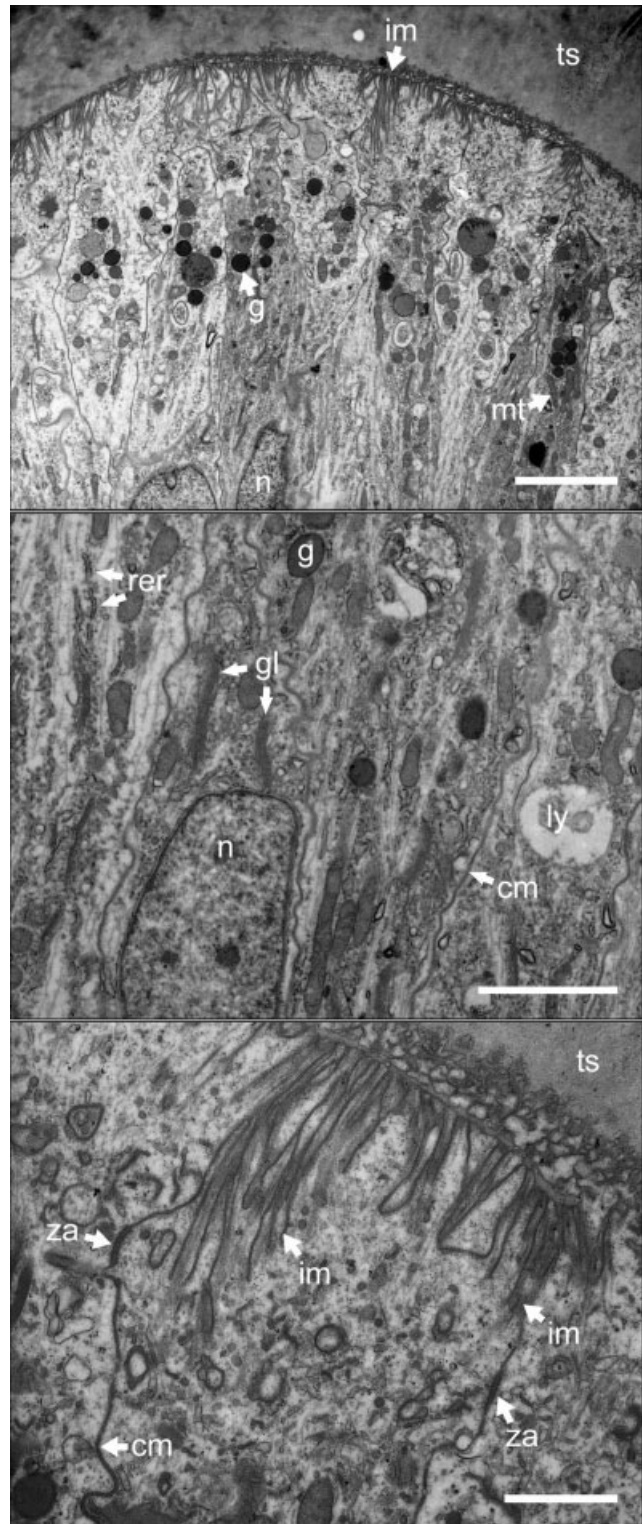


Fig. 5. Ultrastructure of *Acanthopleura hirtosa* epithelial cells at the distal end of the stylus canal. cm, cell membrane; gl, golgi bodies; g, granule; im, interdigitating membranes; ly, lysosome; mt, mitochondria; n, nuclei; rer, rough endoplasmic reticulum; ts, tooth stylus; za, zonula adherens. Scale bars = 2 μ m.

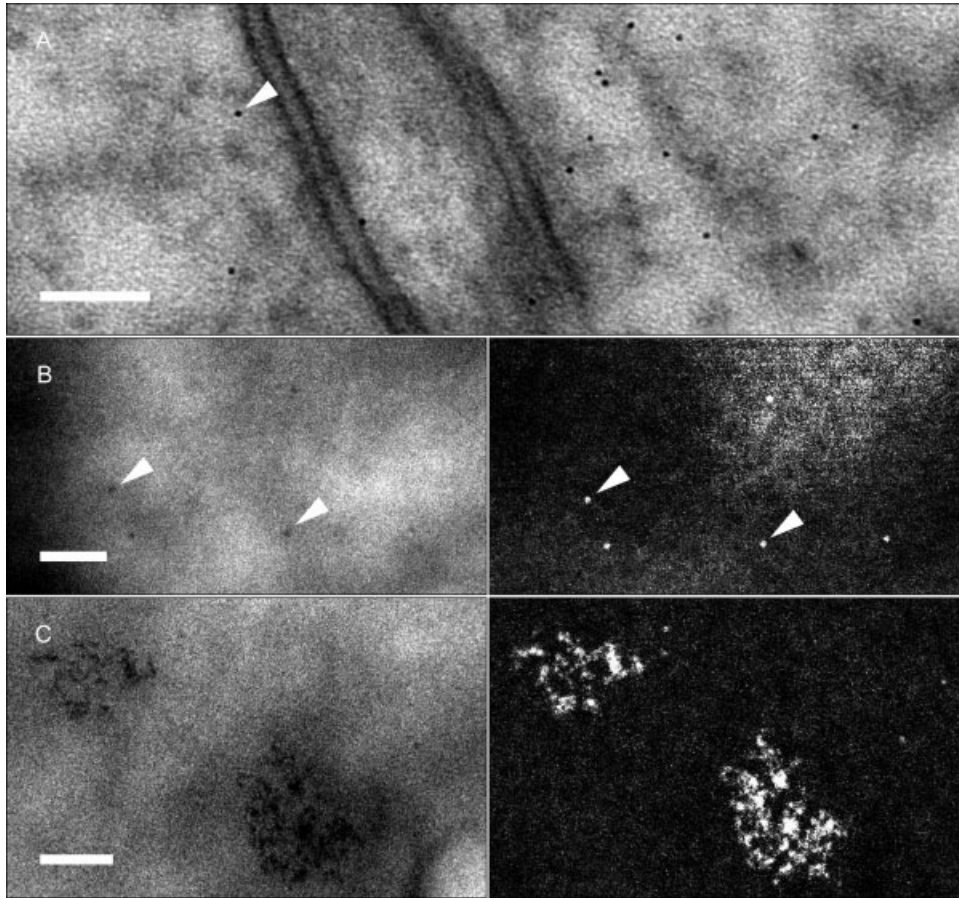


Fig. 6. **A:** Individual 8 nm electron dense particles (arrowheads) within *Acanthopleura hirtosa* stylus canal tissue. **B:** The bright-field (left) and associated energy-filtered TEM iron map (right) show that these individual particles are composed of iron. **C:** Similarly, aggregations of iron particles are also observed within this tissue. Scale bars = 100 nm.

DISCUSSION

The Stylus Canal

This is the first study directed at resolving the structure and function of the stylus canal in the

major lateral teeth of chitons. The canal is filled with columnar epithelial cells, of similar structure to that documented for the cusp epithelium (Nesson and Lowenstam, 1985; Kim et al., 1989).

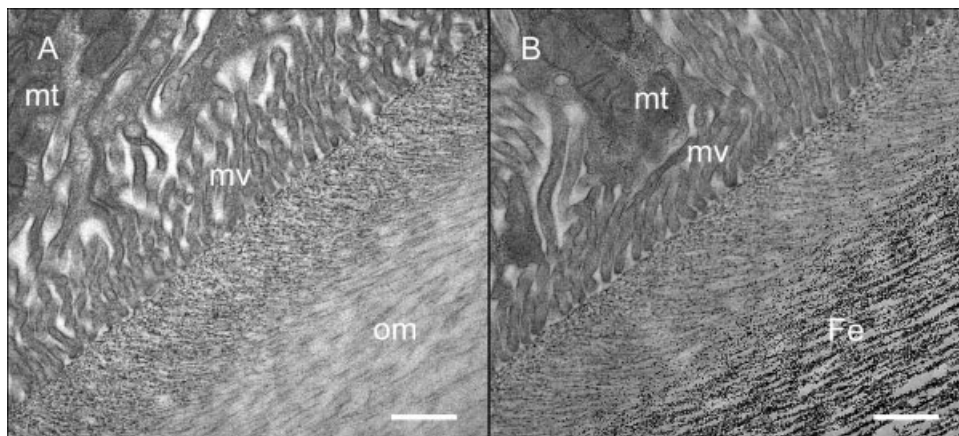


Fig. 7. Bright-field TEM micrographs of the posterior (iron mineralizing) surface of *Acanthopleura hirtosa* tooth cusps (**A**) before mineralization at tooth row 12 and (**B**) at the onset of mineralization at row 13. Note the appearance of iron mineral in association with the tooth organic matrix (om) at row 13. mt, mitochondria; mv, microvilli. Scale bar = 0.5 μm .

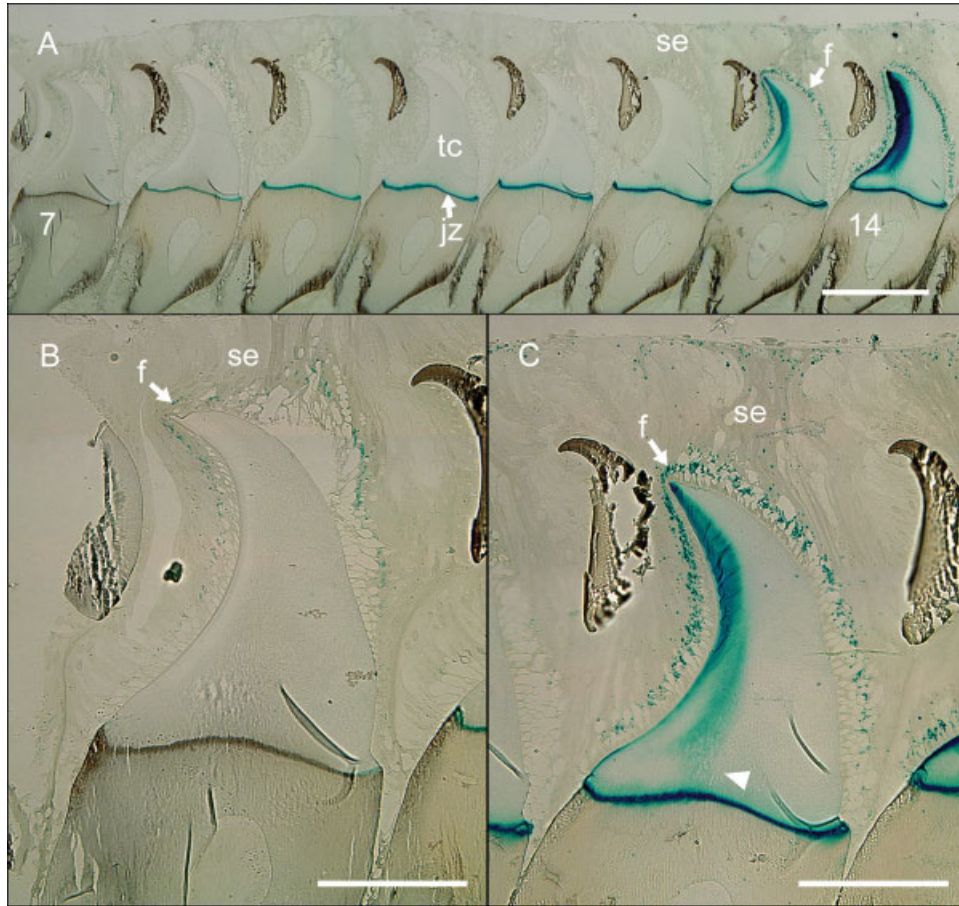


Fig. 8. Tooth cusps and associated superior epithelium from the radula of *Acanthopleura hirtosa* stained with Perl's Prussian blue for ferric iron (Fe^{3+}), showing (A) the distribution of iron in the superior epithelium (se), tooth cusp (tc), and junction zone (jz). Aggregations of iron containing granules (f), identified as ferritin, are evident within the superior epithelium at (B) tooth row 7 and (C) later at tooth row 13, where iron accumulation occurs before the orange tooth at row 14. Also note the presence, in C, of a plume of intensified iron staining within the tooth core above the junction zone at row 13 (white arrowhead). Scale bars = (A) 200 μm and (B and C) 100 μm .

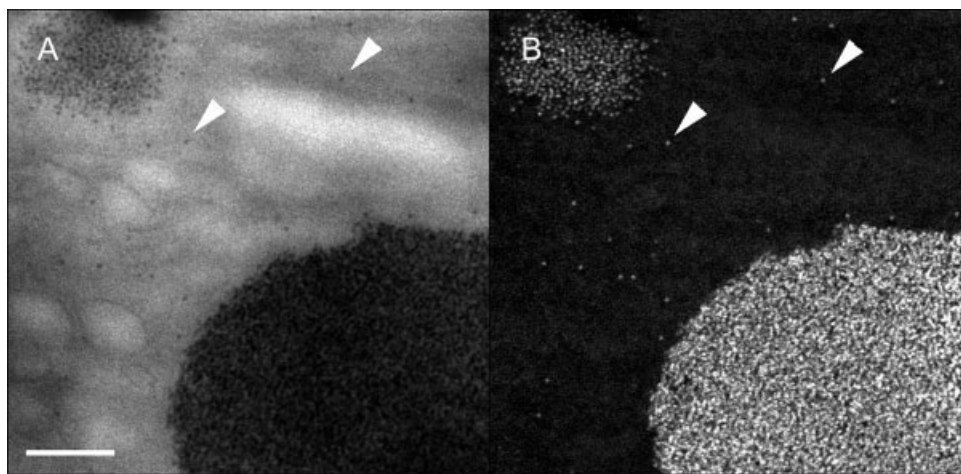


Fig. 9. Bright field and energy-filtered TEM micrographs of isolated 8 nm iron particles (arrowheads) situated between two ferritin siderosomes within the superior epithelial tissue surrounding the major lateral tooth cusps from *Acanthopleura hirtosa*. A: Bright-field image. B: Energy-filtered TEM iron map. Scale bar = 200 nm.

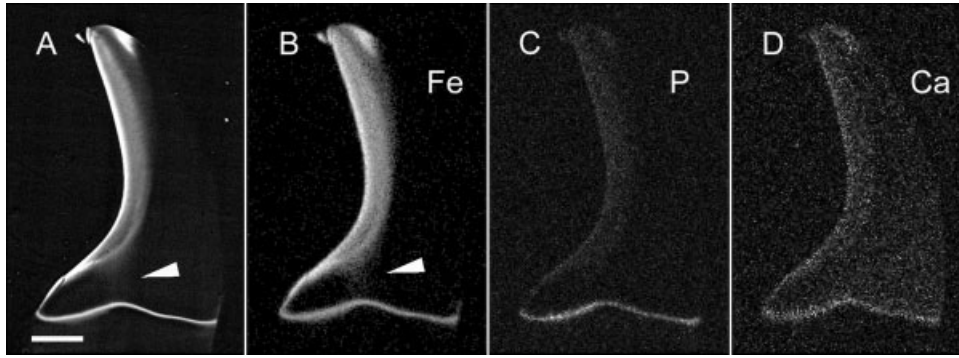


Fig. 10. Tooth row 15 from the radula of *Acanthopleura hirtosa*, showing the presence of a plume (arrowheads) of material in both the (A) back-scatter image and (B) EDS iron element map, which extends from the junction zone toward the iron mineralizing region at the posterior cusp face. The other major mineralizing elements (C) phosphorous and (D) calcium are also present in the junction zone and tooth cusp. Scale bar = 50 μm .

In particular, the apical end of each canal cell possesses interdigitating membranes similar to those found in the cells surrounding the major lateral tooth cusps. This, together with the discovery of iron containing granules within the canal tissue, strongly suggests that the function of the stylus canal is to deliver iron, and possibly other elements, to the junction zone for later delivery into the tooth cusps.

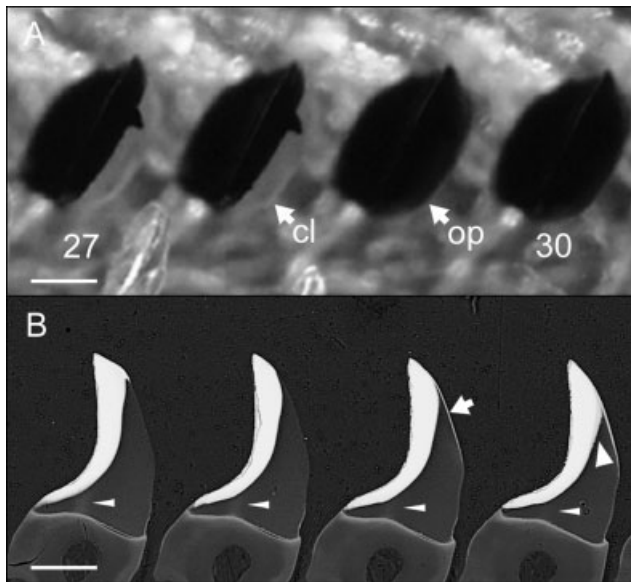


Fig. 11. Developmental changes to the anterior surface of the major lateral tooth cusps from *Acanthopleura hirtosa* at tooth rows 28 and 29. The (A) light micrograph shows the transition from clear (cl) to opaque (op), while the (B) back-scattered SEM image of the same radula in longitudinal section indicates the appearance of high atomic weight elements in this region at row 29 (arrow). Note the presence of the plume (narrow arrowheads) from rows 27 to 30 and the initial formation of the lepidocroite region at row 30 (wide arrowhead). Scale bars = 100 μm .

In addition to *Acanthopleura hirtosa*, the presence of a stylus canal within the major lateral teeth has been confirmed in a further 18 chiton species; representative of many families within the order Chitonida and one species from the order Lepidopleurida (see Table 1). This presence of the stylus canal across the two extant orders of the Polyplacophora (Sirenko, 2006), strongly suggests that it is a structure common to all living representatives of this class of molluscs. The fact that the canal was found only in the major lateral teeth, independent of the body size of the adults of the species, or the size of their teeth, suggests that it plays a major functional role in biomineralization of these teeth. An equivalent structure has not been documented in any other molluscan group (Fretter and Graham, 1962; Hickman, 1977; Messenger and Young, 1999). Patellogastropods (limpets) also exhibit similar patterns of mineralization to chitons, although the iron-oxide goethite is used in conjunction with silica ($\text{SiO}_2 \cdot n\text{H}_2\text{O}$) to mineralize their teeth (Jones et al., 1935; Runham et al., 1969; Liddiard et al., 2004). As in chitons, the initial influx of iron also occurs at the junction zone in limpets (Liddiard et al., 2004; Sone et al., 2007). However, a structure similar to the stylus canal has not yet been described in this group of molluscs.

Cusp Mineralization

The discovery of a plume of elements situated directly over the distal end of the stylus canal provides additional evidence for a function related to cusp mineralization. The presence of the plume also provides the first direct evidence that, in chitons, mineral precursors are transferred into the tooth cusp from the junction zone following the initial accumulation of precursor elements in this region (Macey and Brooker, 1996). In support of

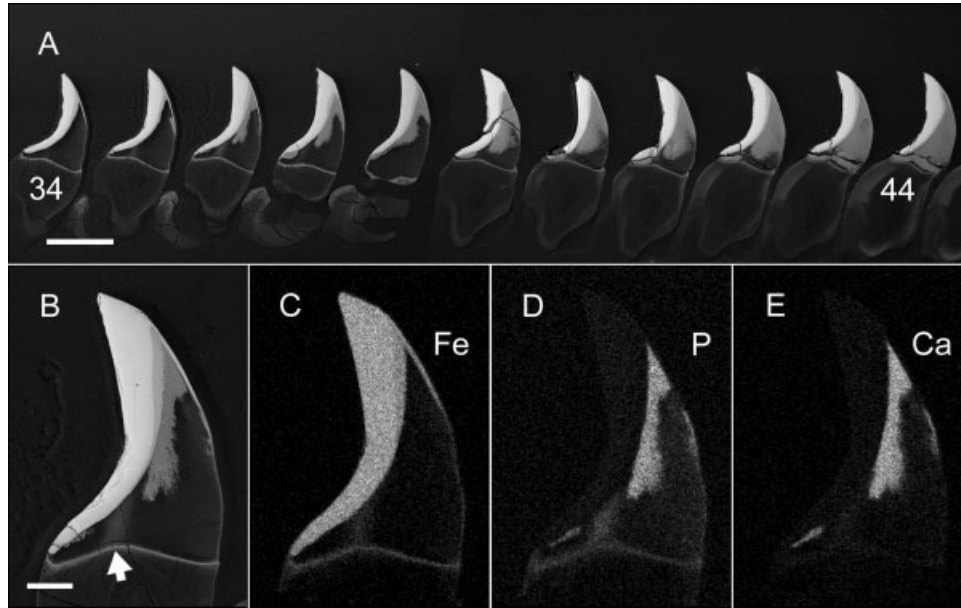


Fig. 12. Initial stages of core mineralization in the major lateral tooth cusps from rows 34 to 44 in *Acanthopleura hirtosa*. **A**: The back-scattered image highlights the progressive infilling of mineral from the apex of the core region, along the anterior surface of the lepidocrocite layer and finally the anterior core region to the junction zone. Note that the plume region remains free of mineral throughout much of the process. The plume (arrow) is clearly evident in the **(B)** back-scattered and **(C-E)** iron, phosphorous, and calcium EDS element maps during core mineralization. Scale bars = **(A)** 200 μm and **(B)** 50 μm .

this, a previous study on the chiton *A. echinata*, using Raman spectroscopy, could not identify mineral phases within the junction zone (Brooker et al., 2003), reinforcing the suggestion that this region has a role in element accumulation and transfer.

Tooth row 13 appears to be pivotal in the mineralization process, as evidenced by the dramatic increase in the number of siderosomes within the cusp epithelium, the initiation of plume formation, and the initial formation of iron crystals on the organic matrix. This coordinated influx of mineralizing elements from the junction zone, as well as from the superior epithelial tissue, would be particularly advantageous for rapidly attaining ion supersaturation within the tooth cusp, a crucial factor for initiating and stabilizing crystal precipitation (Mann, 2001). This combined approach would also facilitate mineralization of the magnetite region from two fronts, a process previously described in the magnetite region of the major lateral teeth of the chiton *A. echinata* (Brooker et al., 2003). Although the plume was not reported in that study, these authors demonstrated that the iron concentration was greater on the internal mineralizing front than that found at the cusp face. The only way for this to be achieved is if there is an internal supply of mineralizing ions from the junction zone.

While the supply of iron for this multiple front mineralization is likely to derive in part from the epithelium on the anterior and posterior cusp surfaces, this model does not account for the deposi-

tion of other minerals into the core region, which only occurs after iron deposition is largely complete thus effectively blocking these pathways (Brooker et al., 2003). In addition, certain chiton species, such as *Ischnochiton australis* and *Plaxiphora albida*, deposit magnetite over both the anterior and posterior surfaces of the tooth cusp before core mineralization, leaving only a small window for the passage of mineralizing elements on the anterior face of the cusp near the junction zone (Macey et al., 1996; Brooker and Macey, 2001). As such, the stylus canal may not only play a significant role in the initial delivery of iron to the mineralizing tooth via the junction zone but may also be responsible for the delivery of phosphorous and calcium to the tooth core during later stages of cusp development. To date, much of the focus has been on the movement of iron, and nothing is known about the accumulation pathways and precipitation for phosphorous and calcium.

Additionally, the organic matrix fibers located between the distal tip of the stylus canal and the tooth cusp are oriented differently from the surrounding matrix material. These structural differences coincide with the location where elements move between the stylus canal and junction zone, and therefore are likely to facilitate the movement of elements, while in some way simultaneously inhibiting crystal precipitation within this region. This is consistent with previous studies on *A. hirtosa*, which have shown differences in matrix structure at the vertical boundary between the

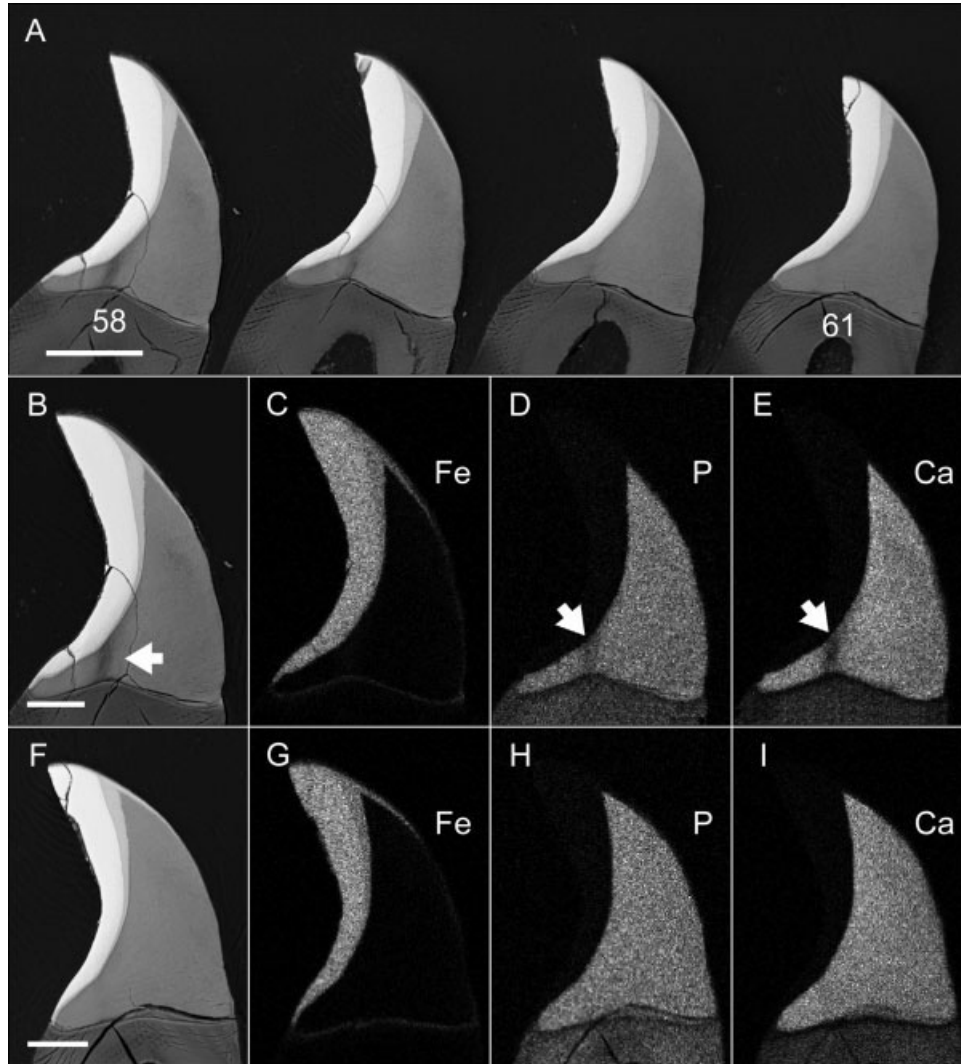


Fig. 13. **A**: Major lateral tooth rows 58 to 61 from *Acanthopleura hirtosa*, highlighting the final stages of core mineralization within the plume region. At row 58, the **(B)** back-scatter and **(C–E)** iron, phosphorous, and calcium EDS elemental maps show low counts of these elements within the plume region (arrows) relative to the remainder of the tooth core. **F–I**: A similar series of images taken at row 61, reveal the final in-filling of this region with phosphorous and calcium. Scale bars = **(A)** 100 μm and **(B and F)** 50 μm .

magnetite and apatite regions of the tooth (Evans et al., 1990, 1994). Fibers in this region were shown to be tightly interwoven, while the mineral component is resistant to acid treatment, suggesting different physical and/or chemical properties to the remainder of the tooth cusp. In addition, immature and demineralized tooth cusps from *A. hirtosa* were shown to retain ferritin in this region in preference to other regions of the cusp (Evans et al., 1994).

The onset of apatite mineralization in *A. hirtosa* occurs at a precise point along the radula, and appears to coincide with the completion of iron deposition, which is consistent with mineralization patterns found in other species (Macey and Brooker, 1996; Lee et al., 2000; Brooker and

Macey, 2001; Brooker et al., 2003). Importantly, in *A. hirtosa*, the final stage of mineral deposition within the tooth core occurs within the plume region, a process that could only be facilitated by a supply of elements from the junction zone. Initially, both phosphorous and calcium are deposited at the apex of the core region, with the mineralization front progressing ventrally over subsequent tooth rows. A similar pattern of core mineralization was described for *A. echinata*, although in this species, final core mineralization was observed toward the anterior tooth surface, above the junction zone (Lee et al., 2000). It is possible that the presence, and therefore final infilling, of the plume region in *A. echinata* was missed due to differences in sample orientation, as the teeth must be aligned

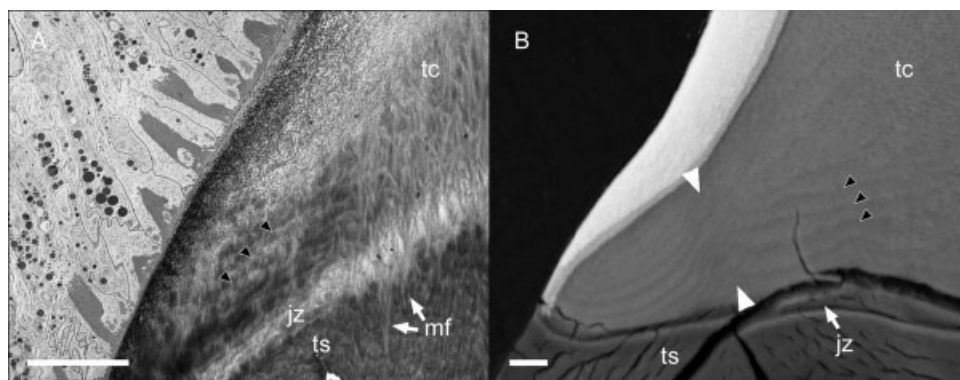


Fig. 14. The plume region above the stylus canal in major lateral teeth from *Acanthopleura hirtosa* imaged at (A) row 17 using TEM and (B) row 61 using back-scattered SEM. In both images, the substructure of the tooth, seen as a series of concentric bands (black arrowheads), is interrupted in the plume region (white arrowheads). The TEM image also shows connectivity of matrix fibers (mf) between the tooth stylus (ts), junction zone (jz), and tooth cusp (tc) in the plume region. Scale bars = (A) 10 μm and (B) 20 μm .

such that the sagittal plane of the cusp, above the stylus canal, is exposed.

The highly sequential delivery of mineralizing elements, together with evidence for the existence of distinct pathways within the cusps, suggest that tooth biomineralization in chitons may be more highly regulated than previously considered. The composite nature of the tooth cusp, with its various mineral regions, can be attributed to the supply of elements delivered not only by the superior epithelium but also from the junction zone, which acts to sustain the mineralization process despite the substantial mineral deposits that eventually cover the anterior and posterior surfaces. At this time, the mechanisms of element movement from the junction zone and epithelium into the tooth cusp are poorly understood. Future studies should focus on the pathways involved in the storage of mineralizing elements at the junction zone and their subsequent distribution into the cusp. In particular, the pathways involved in the initial accumulation of elements at the junction zone are yet to be identified. Such studies will be crucial for our wider understanding of the physiological and biochemical controls over the biomineralization process in this complex system.

ACKNOWLEDGMENTS

The authors acknowledge the facilities, scientific and technical assistance of the Australian Microscopy and Microanalysis Research Facility at the Centre for Microscopy, Characterization and Analysis, The University of Western Australia, a facility funded by The University, State and Commonwealth Governments. The authors thank Mr. Gordon Thomson at Murdoch University for his advice on histological preparations.

LITERATURE CITED

- Brooker LR, Macey DJ. 2001. Biomineralization in chiton teeth and its usefulness as a taxonomic character in the genus *Acanthopleura* Guilding, 1829 (Mollusca: Polyplacophora). *Am Malacol Bull* 16:203–215.
- Brooker LR, Lee AP, Macey DJ, van Bronswijk W, Webb J. 2003. Multiple-front iron-mineralisation in chiton teeth (*Acanthopleura echinata*: Mollusca: Polyplacophora). *Mar Biol* (Berlin) 142:447–454.
- Brydson R. 2001. *Electron Energy Loss Spectroscopy*. Telos: Springer-Verlag. 160p.
- Culling CFA. 1974. *Handbook of Histopathological and Histochemical Techniques (Including Museum Techniques)*. London: Butterworths. 712 p.
- Evans LA, Macey DJ, Webb J. 1990. Characterization and structural organization of the organic matrix of the radula teeth of the chiton *Acanthopleura hirtosa*. *Philos Trans R Soc Lond B Biol Sci* 329:87–96.
- Evans LA, Macey DJ, Webb J. 1994. Matrix heterogeneity in the radular teeth of the chiton *Acanthopleura hirtosa*. *Acta Zool* 75:75–79.
- Fretter V, Graham A. 1962. *British Prosobranch Molluscs, Their Functional Anatomy and Ecology*. London: Ray Society. 755 p.
- Hanaichi T, Sato T, Iwamoto T, Malavasi-Yamashiro J, Hoshino M, Mizuno N. 1986. A stable lead by modification of Sato's method. *J Electron Microsc (Tokyo)* 35:304–306.
- Hickman CS. 1977. Integration of electron scan and light imagery in study of molluscan radulae. *Veliger* 20:1–8.
- Jones EI, McCance RA, Shackleton LRB. 1935. The role of iron and silica in the structure of the radular teeth of certain marine molluscs. *J Exp Biol* 12:59–64.
- Kim KS, Macey DJ, Webb J, Mann S. 1989. Iron mineralization in the radula teeth of the chiton *Acanthopleura hirtosa*. *Proc R Soc Lond B Biol Sci* 237:335–346.
- Lee AP, Brooker LR, Macey DJ, van Bronswijk W, Webb J. 2000. Apatite mineralization in teeth of the chiton *Acanthopleura echinata*. *Calcif Tissue Int* 67:408–415.
- Lewin A, Moore GR, Le Brun NE. 2005. Formation of protein-coated iron minerals. *Dalton Trans* 22:3597–3610.
- Liddiard KJ, Hockridge JG, Macey DJ, Webb J, van Bronswijk W. 2004. Mineralisation in the teeth of limpets *Patelloida alticostata* and *Scutellastra laticostata* (Mollusca: Patellogastropoda). *Molluscan Res* 24:21–31.
- Lowenstam HA. 1962. Magnetite in denticle capping in recent chitons (Polyplacophora). *Geol Soc Amer Bull* 73: 435–438.

- Macey DJ, Brooker LR. 1996. The junction zone: Initial site of mineralization in radula teeth of the chiton *Cryptoplax striata* (Mollusca: Polyplacophora). *J Morphol* 230:33–42.
- Macey DJ, Brooker LR, Webb J, St. Pierre TG. 1996. Structural organization of the cusps of the radular teeth of the chiton *Plaxiphora albida*. *Acta Zool* 77:287–294.
- Mann S. 2001. Biomineralization, Principals and Concepts in Bioinorganic Materials Chemistry. In: Compton, RG, Davies, SG, Evans, J, editors. Oxford: Oxford University Press. 198 p.
- Messenger JB, Young JZ. 1999. The radular apparatus of cephalopods. *Philos Trans R Soc Lond B Biol Sci* 354:161–182.
- Nesson MH, Lowenstam HA. 1985. Biomineralization processes of the radula teeth of chitons. In: Kirshvink JL, Jones DS, MacFadden BJ, editors. Magnetite Biomineralization and Magnetoreception in Organisms. New York: Plenum Press. pp 333–361.
- Runham NW, Thornton PR. 1967. Mechanical wear of the Gastropod radula: A scanning electron microscope study. *J Zool* 154:445–452.
- Runham NW, Thornton PR, Shaw DA, Wayte RC. 1969. The mineralization and hardness of the radular teeth of the limpet *Patella vulgata* L. *Z Zellforsch Mikrosk Anat* 99:608–626.
- Shaw JA, Macey DJ, Brooker LR. 2008a. Radula synthesis by three species of iron mineralizing molluscs: Production rate and elemental demand. *J Mar Biol Assoc UK* 88:597–601.
- Shaw JA, Macey DJ, Clode PL, Brooker LR, Webb RI, Stockdale EJ, Binks RM. 2008b. Methods of sample preparation of epithelial tissue in chitons (Mollusca: Polyplacophora). *Am Malacol Bull* 25:35–41.
- Sirenko B. 2006. New outlook on the system of chitons (Mollusca: Polyplacophora). *Venus* 65:27–49.
- Sone ED, Weiner S, Addadi L. 2007. Biomineralization of limpet teeth: A cryo-TEM study of the organic matrix and the onset of mineral deposition. *J Struct Biol* 158:428–444.
- van der Wal P, Giesen H, Videler J. 2000. Radular teeth as models for the improvement of industrial cutting devices. *Mater Sci Eng C* 7:129–142.